

# Truncated Disks in TW Hya Association Multiple Star Systems

Sean M. Andrews<sup>1,2</sup>, Ian Czekala<sup>1,3</sup>, D. J. Wilner<sup>1</sup>,  
Catherine Espaillat<sup>1,4</sup>, C. P. Dullemond<sup>5</sup>, and A. M. Hughes<sup>1</sup>

## ABSTRACT

We present high angular resolution (down to  $0''.3 \approx 13$  AU in diameter) Submillimeter Array observations of the  $880 \mu\text{m}$  (340 GHz) thermal continuum emission from circumstellar dust disks in the nearby HD 98800 and Hen 3-600 multiple star systems. In both cases, the dust emission is resolved and localized around one stellar component – the HD 98800 B and Hen 3-600 A spectroscopic binaries – with no evidence for circum-system material. Using two-dimensional Monte Carlo radiative transfer calculations, we compare the SMA visibilities and broadband spectral energy distributions with truncated disk models to empirically locate the inner and outer edges of both disks. The HD 98800 B disk appears to be aligned with the spectroscopic binary orbit, is internally truncated at a radius of 3.5 AU, and extends to only 10-15 AU from the central stars. The Hen 3-600 A disk is slightly larger, with an inner edge at  $\sim 1$  AU and an outer radius of 15-25 AU. These inferred disk structures compare favorably with theoretical predictions of their truncation due to tidal interactions with the stellar companions.

*Subject headings:* circumstellar matter — planetary systems: protoplanetary disks — stars: pre-main sequence — binaries: spectroscopic — binaries: visual

## 1. Introduction

A large fraction of the stars in the solar neighborhood are members of gravitationally bound multiple systems (Abt & Levy 1976; Duquennoy & Mayor 1991; Lada 2006). Similar or higher multiplicity fractions are found in nearby young stellar associations (Ghez et al. 1993; Leinert et al. 1993; Simon et al. 1995), confirming that multiplicity is a common outcome in any star formation environment. With such a substantial number of stars residing in multiple systems, it is natural to also consider the potential impacts of stellar companions on the planet formation process. The

---

<sup>1</sup>Harvard-Smithsonian Center for Astrophysics, 60 Garden St., Cambridge, MA 02138; sandrews@cfa.harvard.edu

<sup>2</sup>Hubble Fellow

<sup>3</sup>University of Virginia Department of Astronomy, P. O. Box 400325, Charlottesville, VA 22904

<sup>4</sup>NSF Astronomy & Astrophysics Postdoctoral Fellow

<sup>5</sup>Max Planck Institut für Astronomie, Königstuhl 17, 69117 Heidelberg, Germany

structures of the circumstellar disks used to build planets can be strongly affected by tidal interactions with the stellar components in these systems (Lin & Papaloizou 1993; Artymowicz & Lubow 1994; Pierens & Nelson 2008). These interactions can open gaps in disks, truncate their edges, and potentially expedite their dissipation before planetesimals can be made. But remarkably, despite these formidable dynamical hazards, a relatively large fraction ( $\sim 25\%$ ) of exoplanet host stars have stellar companions (Raghavan et al. 2006; Desidera & Barbieri 2007, and references therein). Observations of circumstellar material in young multiple star systems can be used to empirically characterize the impact of these tidal interactions on disk structures, and therefore to place constraints on when and where planet formation can potentially be accommodated in the presence of a stellar companion.

The fate of the circumstellar material in a young multiple star system is primarily dependent on the orbital separation ( $a$ ), eccentricity ( $e$ ), and mass ratio ( $\mu$ ) of the stellar components (Artymowicz & Lubow 1994). Systems with large separations ( $a \sim$  hundreds of AU) impart little or no dynamical effects on their circumstellar material, leaving disks around each stellar component that are similar to those around single stars. Conversely, individual disks in a small-separation system ( $a \sim$  a few AU or less) will likely not survive. Instead, these systems can host a single circum-system disk with a dynamically cleared central cavity out to a radius comparable to the stellar separation ( $\sim 2-3a$ ). Qualitatively, such theoretical predictions have been broadly supported by observations. The disks around small-separation spectroscopic binaries are like those around single stars except for a diminished dust emission signal shortward of  $\sim 5 \mu\text{m}$ , consistent with a lack of warm material inside a few AU (Jensen & Mathieu 1997). Likewise, disks in wide binary systems are comparable to their more isolated counterparts, although the secondary disk signatures are often weak or absent (e.g., Jensen & Akeson 2003; Andrews & Williams 2005a; Patience et al. 2008).

But most multiple systems in both the field and young clusters have orbits with intermediate separations ( $a \sim$  tens of AU; e.g., Mathieu et al. 2000). The disks in these systems suffer the most dramatic effects of star-disk interactions, resulting in their external truncation at a fraction of the component separation ( $\sim 0.2-0.5a$ ), or perhaps their complete dispersal. Single-dish radio photometry surveys have demonstrated that the  $\sim 1$  mm luminosities for medium-separation binaries are significantly lower than their more closely or widely separated counterparts (as well as single stars; Jensen et al. 1994, 1996a; Osterloh & Beckwith 1995; Andrews & Williams 2005b). Since the dust emission at these wavelengths is optically thin (Beckwith et al. 1990), this luminosity deficit is interpreted as indirect evidence for a diminished disk mass due to the tidal truncation of the outer disk. However, this *total mass* deficit does not necessarily have any bearing on the potential for making planets around medium-separation multiples. The likelihood for planet formation depends more on reaching a critical disk *density*, and therefore it is more important to identify how that total mass is distributed spatially in such systems. Doing so involves locating where the disks in multiple star systems are truncated using high angular resolution observations of their millimeter continuum emission (e.g., Jensen et al. 1996b; Akeson et al. 1998; Guilloteau et al. 1999, 2008).

In this article, we present the first set of high angular resolution millimeter observations of the circumstellar material in two nearby multiple star systems, HD 98800 and Hen 3-600. Both systems are members of the TW Hya association and are therefore among the nearest pre-main sequence stars, with a distance of roughly 50 pc (Kastner et al. 1997; Webb et al. 1999). HD 98800 is a rare quadruple star system, consisting of a pair of spectroscopic binaries with  $\sim 1$  yr periods separated by  $0''.8$  (36 AU) on the sky (e.g., Torres et al. 1995; Tokovinin 1999). Infrared measurements have shown that only the HD 98800 B system harbors a circumstellar dust disk (Koerner et al. 2000; Prato et al. 2001), which appears to have a nearly empty central cavity out to a few AU in radius (Furlan et al. 2007). The coronal X-ray line ratios and very weak H $\alpha$  emission observed from HD 98800 B suggest that the stars are not actively accreting gas from the disk (Kastner et al. 2004; Dunkin et al. 1997). Hen 3-600 appears to be a hierarchical triple star system, comprised of a primary spectroscopic binary of uncertain period (Muzerolle et al. 2000; Torres et al. 2003) and a secondary visual companion located  $1''.5$  (66 AU) to the southwest (de la Reza et al. 1989). The signatures of a circumstellar disk, including spectroscopic and X-ray line ratio evidence for accretion onto the central stars, have been identified around the Hen 3-600 A spectroscopic binary (e.g., Jayawardhana et al. 1999; Muzerolle et al. 2000; Huenemoerder et al. 2007).

At their advanced ages of  $\sim 10$  Myr, the nature of the circumstellar material in these low-mass pre-main sequence systems is a topic of active debate. While the accretion signatures in the Hen 3-600 A disk are supportive of a primordial reservoir, it is unclear whether the HD 98800 B disk contains gas or has evolved into a debris-only system (see the detailed discussion on this topic by Akeson et al. 2007). Regardless, the proximity of these systems offers unusually detailed views of their circumstellar structures. We aim to use the high spatial resolution afforded by that proximity to characterize how the disk structures have been shaped by their dynamical interactions with the stellar components in each system. We present our observations in §2 and a brief qualitative analysis of the data in §3. We discuss the radiative transfer modeling used to determine the disk structures in §4, and synthesize the results with theoretical predictions for disk truncation in §5.

## 2. Observations and Data Reduction

The HD 98800 and Hen 3-600 systems were observed with the Submillimeter Array interferometer (SMA; Ho et al. 2004) at Mauna Kea, Hawaii in the compact (baselines of 16-70 m), extended (baselines of 28-226 m), and very extended (baselines of 68-509 m) configurations on 2008 March 9, February 21, and April 3, respectively. The SMA double-sideband receivers were tuned with a local oscillator (LO) frequency of 340.755 GHz (880  $\mu$ m). Each sideband provides 24 partially overlapping 104 MHz spectral chunks centered  $\pm 5$  GHz from the LO frequency. The correlator was configured to subdivide one chunk in each sideband into 128 spectral channels to sample any emission from the CO  $J=3-2$  transition (345.796 GHz) at a velocity resolution of 0.7 km s $^{-1}$ . Each of the remaining chunks was split into 32 coarser spectral channels to observe continuum emission.

The observations cycled through the two targets and TW Hya (Andrews et al., *in preparation*)

between integrations on the nearby quasar J1037–295, with a total cycle time of 18 minutes (5 minutes per each disk target, 3 minutes on the quasar) in the compact and extended configurations and 12 minutes (3 minutes for each disk target and quasar) in the very extended configuration. The bright quasar 3C 279 was observed every other cycle to help assess the quality of phase transfer. Additional observations of bright quasars (3C 84, 3C 273, 3C 279, and 3C 454.3) and Callisto were made for bandpass and absolute flux calibration when the targets were at low elevations ( $<20^\circ$ ). The observing conditions were excellent, with zenith opacities ranging from 0.04–0.08 (corresponding to 0.8–1.6 mm of precipitable water vapor) and well-behaved phase variations on timescales longer than the calibration cycle. The extended array observations (2008 February 21) were conducted during a configuration change, and therefore only utilized 4 of the 8 SMA antennas.

The data were edited and calibrated with the MIR software package.<sup>1</sup> The bandpass response was calibrated with observations of bright quasars, and broadband continuum channels in each sideband were generated by averaging the central 82 MHz in all coarse resolution spectral chunks. The visibility amplitude scale was set by bootstrapping quasar flux densities from the observations of Callisto. The absolute flux calibration uncertainty from this technique is estimated to be roughly 10%. The antenna-based complex gain response of the system as a function of time and elevation was determined with reference to the observations of J1037–295 (the nearest sufficiently bright calibrator), located midway between and  $\sim 10^\circ$  from each of the science targets. The phase transfer between the calibrator and science targets over that angular separation is not ideal, especially given the low observing elevations for these southern systems. Atmospheric decoherence on these scales will add phase noise that acts to smear out the emission from the targets. Typically, observations of a second quasar are utilized to estimate the level of decoherence in terms of the size of the “seeing” disk. Unfortunately, the next nearest bright quasar, 3C 279, probes the atmosphere at a much larger 30–40° separation from the targets. Nevertheless, the observations of 3C 279 were used to estimate the quality of phase transfer in an extreme case and showed a seeing disk size of  $\sim 0''.3$ . The actual phase decoherence between the targets and J1037–295 should be much less severe, producing significantly smaller (but still uncertain) seeing disks.

After the gain calibration, the independent sets of visibilities from each configuration and sideband were compared to check for consistency on overlapping spatial scales. After finding excellent agreement, all of the data for each target were combined. The standard tasks of Fourier inverting the visibilities, deconvolution with the CLEAN algorithm, and restoration with a synthesized beam were conducted with the MIRIAD package. Maps of the continuum and CO  $J=3-2$  line emission were made by naturally weighting the visibilities. The resulting continuum maps have  $1\sigma$  rms noise levels of  $3.5 \text{ mJy beam}^{-1}$ , with synthesized beam dimensions of  $0''.92 \times 0''.68$  at a position angle (PA, measured east of north) of  $11^\circ$  for HD 98800 and  $1''.11 \times 0''.74$  at PA =  $18^\circ$  for Hen 3-600. To maximize the sensitivity to line emission, only data from the compact configuration were used to generate CO  $J=3-2$  spectral images, with synthesized beam dimensions of  $3''.1 \times 1''.8$  at PA =

---

<sup>1</sup>See <http://cfa-www.harvard.edu/~simscqi/mircook.html>.

$164^\circ$  and  $4''.0 \times 1''.8$  at  $\text{PA} = 168^\circ$  for HD 98800 and Hen 3-600, respectively. No line emission was detected for either target, with  $3\sigma$  upper limits of  $\sim 0.6 \text{ Jy beam}^{-1}$  in a  $0.7 \text{ km s}^{-1}$  channel.

### 3. Results

The synthesized images of the  $880 \mu\text{m}$  (340 GHz) dust continuum emission in the HD 98000 and Hen 3-600 systems are shown in Figure 1. The HD 98800 map exhibits emission with an integrated flux density of 110 mJy and peak of  $82 \pm 3 \text{ mJy beam}^{-1}$ , centered at  $\alpha = 11^{\text{h}}22^{\text{m}}05^{\text{s}}.24$ ,  $\delta = -24^\circ 46' 39''.10$  (J2000). Based on the reference coordinates and proper motion estimates from *Hipparcos* (which resolved the HD 98800 A-B system; Perryman et al. 1997), the SMA emission centroid is coincident with the HD 98800 B spectroscopic binary position to within  $\sim 50 \text{ mas}$ , well below the SMA astrometric uncertainty of  $\sim 0''.1$  (and roughly on the scale of the Ba-Bb separation). The location of the HD 98800 A spectroscopic binary is marked on Figure 1 with a star symbol  $0''.8$  to the south of the map center. The Hen 3-600 system shows emission with an integrated flux density of 75 mJy and peak of  $57 \pm 3 \text{ mJy beam}^{-1}$ , centered at  $\alpha = 11^{\text{h}}10^{\text{m}}27^{\text{s}}.84$ ,  $\delta = -37^\circ 31' 51''.71$  (J2000). Using the *Two Micron All Sky Survey* (2MASS) astrometry (Cutri et al. 2003) and the proper motion determined by Torres et al. (2006), we find that the SMA emission centroid is coincident with the Hen 3-600 A spectroscopic binary position to within 15 mas in right ascension and  $0''.15$  in declination (the measured position is offset to the north, away from Hen 3-600 B). Given the astrometric errors that may occur for such a low declination target as well as the potential confusion in the 2MASS catalog astrometry from the close companion, we suggest that the continuum emission measured with the SMA is consistent with being centered on Hen 3-600 A. The location of the Hen 3-600 B companion is marked in Figure 1 with a star symbol  $\sim 1''.5$  to the southwest of the map center.

An examination of the SMA visibilities confirms that the emission from each target is partially resolved (see §4). An elliptical Gaussian fit to the HD 98800 B visibilities indicates an elongated emission morphology, with a high aspect ratio corresponding to an inclination  $i \approx 55\text{-}71^\circ$  at a major axis orientation  $\text{PA} \approx 130\text{-}159^\circ$  east of north. This inferred disk geometry is in excellent agreement with the much more precisely determined orbital geometry of the HD 98800 B spectroscopic binary, for which Boden et al. (2005) have measured  $i = 67^\circ$  and  $\Omega = 338^\circ$  (corresponding to  $\text{PA} = 158^\circ$ ). Within the uncertainties of the SMA data, the HD 98800 B disk and spectroscopic binary orbital plane are aligned. A similar fit to the Hen 3-600 A visibilities suggests a more circular emission morphology, with inclination estimates of  $i \approx 25\text{-}45^\circ$  and a major axis orientation  $\text{PA} \approx 145\text{-}185^\circ$  east of north. Lacking orbital information for either the spectroscopic binary or the wider visual pair, the relative orientation of the star and disk axes in this system remains unclear.

#### 4. Disk Models

The 880  $\mu\text{m}$  visibilities presented here provide the first spatially resolved information about the HD 98800 B and Hen 3-600 A circumstellar disks. We aim to use these data to directly locate the outer disk edges, where the circumstellar material could be truncated by tidal interactions with their nearby stellar companions. Moreover, following the analysis of Jensen & Mathieu (1997), we seek to indirectly locate the inner disk edges sculpted by their central spectroscopic binaries based on the high-quality infrared spectra presented by Uchida et al. (2004) and Furlan et al. (2007). To determine these disk edges, we utilize a parametric truncated disk structure model and a two-dimensional Monte Carlo radiative transfer code (RADMC; see Dullemond & Dominik 2004) to compute synthetic 880  $\mu\text{m}$  visibilities and spectral energy distributions (SEDs) that can be compared with observations. A detailed description of the modeling methodology was provided by Andrews et al. (2009), and so here we focus only on the key modifications made to accommodate truncated disk structures.

We parameterize the axisymmetric density structure for the disk models based on two different radial zones, including a standard “outer” disk and a central disk “cavity” that contains substantially less material. The surface densities have a  $\Sigma \propto 1/R$  behavior for  $R_{\text{cav}} \leq R \leq R_{\text{out}}$  in the outer zone, and a constant value (depleted by a factor  $\delta_{\Sigma}$  from the value at  $R_{\text{cav}}$ ) inside the cavity ( $R_{\text{in}} \leq R < R_{\text{cav}}$ ). The vertical density structure is assumed to be Gaussian and is parameterized by a scale-height distribution  $H \propto R^{1+\psi}$  that can be artificially “puffed”-up by a factor  $\delta_H$  at the cavity edge ( $R_{\text{cav}}$ ) to account for the locally increased energy input from the normal irradiation of the optically thick outer disk zone (e.g., Dullemond et al. 2001; D’Alessio et al. 2005). The densities in these structures are normalized with a total dust mass,  $M_{\text{dust}}$ .

We use the same set of dust opacities adopted by Andrews et al. (2009), computed for a power-law size distribution up to a maximum grain radius of 1 mm. For a small fraction,  $f_{\text{sg}}$ , of the dust mass inside the disk cavities, the maximum grain size was decreased to 1  $\mu\text{m}$  (hereafter “small” grains) to more faithfully reproduce the solid-state dust emission features for each target. In these models, we assume the only heating source was irradiation from a central stellar photosphere, represented by appropriately scaled Lejeune et al. (1997) spectral templates that match the component-resolved optical and near infrared photometry (Gregorio-Hetem et al. 1992; Soderblom et al. 1998; Webb et al. 1999; Low et al. 1999; Weintraub et al. 2000; Koerner et al. 2000; Prato et al. 2001; Geoffroy & Monin 2001). Table 1 lists the stellar parameters adopted in the modeling. The corresponding photosphere templates are also used to help construct the complete broadband SEDs for each disk. Since neither the HD 98800 A or Hen 3-600 B components are found to harbor any disk material, we subtract their stellar templates from the composite *Spitzer* IRS spectra for each system (Uchida et al. 2004; Furlan et al. 2007) to derive the star+disk spectra for HD 98800 B and Hen 3-600 A alone. Assuming that the emission at longer wavelengths is generated solely by the disks, we include the far-infrared and millimeter photometry from the literature in the SEDs without any such corrections (Jensen et al. 1996a; Sylvester et al. 1996, 2001; Low et al. 2005).

In this modeling effort, no attempt was made to account for irradiation from individual components of the eccentric spectroscopic binaries or from any *external* disk irradiation by the close stellar companions (e.g., Nagel et al. 2009). For convenience, the updated HD 98800 *Hipparcos* distance of 45 pc was adopted for both systems (van Leeuwen 2007). Note that this kind of parametric modeling is still subject to some intrinsic degeneracies, which have been discussed at length elsewhere (Thamm et al. 1994; Chiang et al. 2001; Andrews & Williams 2007a; Andrews et al. 2009). Some degeneracies specific to this truncated disk structure model are highlighted below. Because the 880  $\mu\text{m}$  emission from the target disks is relatively faint, the exploration of parameter-space was limited. Focus was placed on estimating  $R_{\text{cav}}$  and  $R_{\text{out}}$  for reasonable assumptions about the ranges of other input parameters.

The best estimates for the HD 98800 B and Hen 3-600 A disk structure parameters described above are compiled in Table 2. The observed broadband SEDs and *Spitzer* IRS spectra from the literature are shown in Figure 2, with the composite stellar photosphere spectra overlaid in gray. The best-fit synthetic SEDs for disk models with several fixed values of the outer radius ( $R_{\text{out}}$ ) are plotted for comparison. Neither disk exhibits dust emission in excess of the photosphere at wavelengths less than  $\sim 5 \mu\text{m}$ , as was noted in previous infrared studies (e.g., Jayawardhana et al. 1999; Uchida et al. 2004; Furlan et al. 2007). This lack of excess emission and the secondary emission peak near 20  $\mu\text{m}$  were reproduced in the models by varying the disk cavity parameters,  $\{R_{\text{in}}, R_{\text{cav}}, \delta_{\Sigma}, \delta_H\}$  (and to some extent  $f_{\text{sg}}$ ). Of these, we perhaps have the best handle on  $R_{\text{cav}}$  due to the prominent role it has in shaping the rising mid-infrared spectrum and setting the wavelength of the secondary emission peak. Our estimate of  $R_{\text{cav}} = 1 \text{ AU}$  for the Hen 3-600 A disk is in good agreement with the original measurement from these data by Uchida et al. (2004), but the  $R_{\text{cav}} = 3.5 \text{ AU}$  inferred here for the HD 98800 B disk is somewhat smaller than the 5.9 AU derived by Furlan et al. (2007). Given the differences in the adopted stellar parameters, dust populations, and the prescribed physical structure of the cavity edge between these two studies, this apparent  $R_{\text{cav}}$  discrepancy is probably irrelevant. However, if the cavity extended out to the radius determined by Furlan et al. (2007), we would expect to see a null in the 880  $\mu\text{m}$  visibilities on  $\sim 350\text{-}400 \text{ k}\lambda$  baselines, corresponding to angular scales of  $\sim 0''.3$  (see Hughes et al. 2007). Since no such null is noted in the SMA data (see Figure 3), a smaller cavity size is appropriate.

The additional cavity parameters,  $\{R_{\text{in}}, \delta_{\Sigma}, \delta_H, f_{\text{sg}}\}$ , are not well-constrained and are somewhat mutually degenerate. For example, one could adjust  $R_{\text{in}}$  and compensate for the modified infrared emission by varying  $\delta_{\Sigma}$ . Nevertheless, in practice the range of viable parameter-space is relatively small, and the values selected here are meant only to be illustrative and facilitate reasonable estimates of the disk edges. Both disks contain only a miniscule  $\sim 10^{-10} M_{\odot}$  of dust inside  $R_{\text{cav}}$ , a fraction  $f_{\text{sg}}$  (by mass) of which is comprised of small grains. The scale-height modifications at  $R_{\text{cav}}$  ( $\delta_H$ ) are important, but also modest, amounting to a change from 0.19 to 0.26 AU for HD 98800 B and 0.0026 to 0.0032 AU for Hen 3-600 A. The vertical structure parameters inferred for both disks are similar to their non-truncated counterparts in the Ophiuchus star-forming region (Andrews et al. 2009), but their total dust masses are an order of magnitude smaller than the typi-

cal T Tauri disk (Andrews & Williams 2007b). Note that the Hen 3-600 A disk has a slightly higher  $M_{\text{dust}}$  than HD 98800 B, despite the latter being brighter at  $880 \mu\text{m}$ . The apparent discrepancy is a result of the significantly cooler dust temperatures produced around the later-type Hen 3-600 A stars.

Because there is no spatially resolved information in the SEDs alone, those data can be reproduced equally well with essentially any value for the outer disk edge. Not surprisingly then, the SED models for different  $R_{\text{out}}$  values shown in Figure 2 are practically identical. However, the synthetic  $880 \mu\text{m}$  continuum visibilities computed from the same disk models exhibit distinctive signatures for different outer edge locations. Figure 3 displays the azimuthally-averaged representations of the observed and synthetic visibilities for the HD 98800 B and Hen 3-600 A disks, deprojected to account for the disk viewing geometries (see Lay et al. 1997). The real parts of the SMA visibilities decrease with deprojected baseline, demonstrating that both disks are resolved. Moreover, the imaginary parts of the visibilities are essentially zero, indicating that there is no strong evidence for large departures from axisymmetry. To facilitate a fair comparison of the data and models, the model visibilities are first convolved with a  $0''.15$  Gaussian to compensate for the atmospheric decoherence discussed in §2. After this “seeing” correction, it is clear in Figure 3 that the SMA data are best reproduced for  $R_{\text{out}}$  values of  $\sim 10\text{-}15$  AU for the HD 98800 B disk and  $\sim 15\text{-}25$  AU for the Hen 3-600 A disk. These values could be smaller if the decoherence is under-estimated, but they could only be larger if  $\Sigma$  were a steeper function of radius (see Andrews & Williams 2007a).

## 5. Discussion

Through radiative transfer modeling of resolved  $880 \mu\text{m}$  continuum emission and pan-chromatic spectral energy distributions, we have characterized the key properties of the circumstellar material in two of the nearest pre-main sequence multiple star systems. In principle, the disk structures determined here can be used to help assess the potential for planet formation in the presence of a stellar companion and to test theoretical calculations of star-disk tidal interactions. The latter task has further implications for disk studies, as empirical constraints on these dynamical interactions can be used as high mass ratio ( $\mu$ ) touchstones for modeling the impacts of young giant planet companions on their local disk environments.

Unfortunately, very little is known about the stellar orbits in the Hen 3-600 hierarchical triple system. Muzerolle et al. (2000) noted that the primary appears to be a double-lined spectroscopic binary with a large radial velocity difference ( $\sim 40 \text{ km s}^{-1}$ ), although repeated measurements have not been able to extract a reliable set of orbital parameters (Torres et al. 2003). If the inner truncation radius estimated for the Hen 3-600 A disk,  $R_{\text{cav}} \approx 1 \text{ AU}$ , is indeed set by the dynamical clearing effects of the central spectroscopic binary, the calculations by Artymowicz & Lubow (1994) predict that the orbital separation should be in the range  $a \approx 0.2\text{-}0.6 \text{ AU}$ , depending on the eccentricity (mass ratio-related effects are small when  $\mu \approx 0.1\text{-}0.5$ ). The visual companion Hen 3-600 B has been located at angular separations of  $1.4\text{-}1''.5$  to the southwest ( $\text{PA} \approx 215\text{-}230^\circ$ ) of the spectro-



scopic binary system, corresponding to projected spatial separations of 63-67 AU (de la Reza et al. 1989; Reipurth & Zinnecker 1993; Webb et al. 1999; Brandeker et al. 2003). While there are no available constraints on the A-B orbit, projection effects should only produce up to a  $\sim 20\%$  uncertainty in the physical separation if the disk plane and orbit are aligned. Assuming that the similar spectral types of the A and B components imply a roughly equal-mass system ( $\mu \approx 0.5$ ), tidal interactions would externally truncate the Hen 3-600 A disk at a radius of  $\sim 25$  AU for a circular orbit (Artymowicz & Lubow 1994). The outer disk edge inferred here,  $R_{\text{out}} \approx 15\text{-}25$  AU, is in good agreement with that prediction, with the uncertainty permitting moderate orbital eccentricities.

The stellar orbital parameters in the HD 98800 quadruple system are comparatively more robust, thanks to long-term and intensive monitoring efforts. Most recently, Boden et al. (2005) combined infrared interferometric observations with the extant spectroscopic data from Torres et al. (1995) to measure the orbital elements and individual stellar properties in the HD 98800 B spectroscopic binary. According to the simulations of Pichardo et al. (2008), this nearly equal-mass ( $\mu = 0.43$ ), eccentric ( $e = 0.78$ ), and close ( $a = 1.05$  AU) system can harbor a circumbinary disk with an innermost stable orbit at a radius of  $\sim 3.7$  AU. A similar value can be deduced from the calculations of Holman & Wiegert (1999), or from a slight extrapolation of the results of Artymowicz & Lubow (1994). That value is practically identical to the internal truncation radius determined from the infrared spectrum morphology,  $R_{\text{cav}} = 3.5$  AU. For the wider HD 98800 A-B visual pair, Torres et al. (1995) compiled a relative astrometric record of the resolved system over the past century, along with a single-epoch measurement of the systemic radial velocity difference between the components. With that information and the *Hipparcos* parallax, Tokovinin (1999) determined a family of acceptable A-B orbits with  $\sim 300\text{-}430$  yr periods, moderate eccentricities ( $e = 0.3\text{-}0.6$ ), and  $a \approx 50\text{-}80$  AU. For reference, the relative geometries of the HD 98800 B disk and an example A-B orbit from Tokovinin (1999) are shown together in Figure 4, projected onto the plane of the sky. Note that the A-B orbital plane ( $i \approx 88^\circ$ ,  $\Omega \approx 185^\circ$ ) is not aligned with the B spectroscopic binary and disk plane ( $i \approx 67^\circ$ ,  $\Omega \approx 338^\circ$ ), making a quantitative prediction for the external disk truncation difficult. Although the aforementioned theoretical calculations all assume coplanar interactions, we can use them as a guide to assess whether or not the outer truncation radius determined here is reasonable. Assuming that the A and B spectroscopic binaries are roughly equal in total mass, the models of Artymowicz & Lubow (1994) or Pichardo et al. (2005) predict that the HD 98800 B disk should be truncated at a radius of  $\sim 8\text{-}20$  AU, depending on the assumed disk viscosity and which Tokovinin (1999) orbit is adopted. Those values are indeed consistent with the estimates based on modeling the resolved SMA data, where  $R_{\text{out}} \approx 10\text{-}15$  AU.

In general, the locations of the disk edges derived from our radiative transfer modeling are in good agreement with the theoretical predictions of disk truncation due to star-disk tidal interactions. However, there are some notable problems in the details that should be brought to attention. One of these involves the proper interpretation of the inner disk radius,  $R_{\text{in}}$ , and the small amount of dust between it and the cavity edge ( $R_{\text{cav}}$ ). For the disk models used here, that small dust mass is necessary to reproduce the weak infrared excesses and silicate emission features present in the

observed SEDs. However, the dynamical models suggest that there are no long-term stable dust orbits inside the inferred  $R_{\text{cav}}$ . Perhaps the simplest way of reconciling this discrepancy is to argue that the adopted parameterization of the inner disk structure is inappropriate or incomplete. For example, similar infrared excess features could potentially be reproduced by modifying the dust content, shape, or symmetry of the disk at the cavity edge (e.g., Isella & Natta 2005; Akeson et al. 2007). With the same data for the HD 98800 B disk, Furlan et al. (2007) employed a narrow ring interior to their slightly larger cavity edge to reproduce the infrared spectrum with equivalent accuracy. The ability to obtain quality fits to the observations with such different interior structures highlights the model degeneracies, which will remain until the inner disk edge is spatially resolved.

But if the inner disk structures determined here are taken at face value, the material inferred to be inside the cavity edge could be interpreted as dynamically unstable, perhaps representative of a low-density inward flow due to Poynting-Robertson drag or disk accretion (e.g., see Pierens & Nelson 2008). Furlan et al. (2007) suggested the former mechanism to explain the narrow ring from 1.5-2 AU they inferred in the HD 98800 B system, but rightly acknowledged that the empty region from 2 AU to their  $R_{\text{cav}}$  (5.9 AU) was incompatible with such a flow (note also that a significant fraction of such a ring would be *inside* the spectroscopic binary orbit). The structure parameterization adopted here is continuous from  $R_{\text{cav}}$  inwards to  $R_{\text{in}}$  (which corresponds to the spectroscopic binary apastron distance), and so avoids this complication. Therefore, P-R drag could potentially account for the material inside the stable orbit radius in this disk if there is a continually replenished dust supply near  $R_{\text{cav}}$  and viscous gas drag forces are negligible. At least the latter condition appears to be met for the HD 98800 B disk, where no evidence for accretion or molecular gas has been uncovered (Dent et al. 2005; Salyk et al. 2009). The same is not true for the Hen 3-600 A disk, which exhibits the clear signatures of a  $\dot{M} \approx 5 \times 10^{-11} M_{\odot} \text{ yr}^{-1}$  gaseous accretion flow from the outer disk to the spectroscopic binary (Muzerolle et al. 2000). In this case, the small amount of material inside  $R_{\text{cav}}$  may be tracing dust grains swept up in that flow.

When future astrometric and spectroscopic monitoring has fully determined the visual orbits in the HD 98800 and Hen 3-600 systems, the lack of millimeter emission around the secondaries can also help constrain how their circumstellar material evolved. In principle, the tidal truncation calculations described above predict similar (perhaps slightly smaller) outer edge locations for the disks around the nearly equal-mass secondaries (Artymowicz & Lubow 1994; Pichardo et al. 2005). If the individual disks initially had the same masses, the similar disk sizes would have produced comparable millimeter emission levels from both components. Obviously this is not the case for these targets, nor for a handful of other resolved multiple systems (Jensen & Akeson 2003; Patience et al. 2008). This could be an artifact of the multiple star formation process itself, as Bate & Bonnell (1997) have argued that competitive accretion will produce higher initial disk masses around primary stars (see also Bate 2000). Alternatively, the dynamical interactions in these systems could be considerably more complicated than the standard tidal truncation calculations have assumed, with the secondary disks suffering more severe disruption. For example, the interactions in non-coplanar systems like the HD 98800 A-B visual binary could be catastrophic, producing a much

more complex circumstellar structure (Verrier & Evans 2008).

The Hen 3-600 and HD 98800 multiple star systems should continue to be exploited as essential test cases for evaluating how external dynamical interactions can contribute to disk evolution, and therefore affect the potential for planet formation in the presence of stellar companions. The unique proximity of these particular systems is crucial, providing both high sensitivity and spatial resolution to circumstellar dust structures as well as rare opportunities to determine precise orbits for stellar pairs with different separations within the same system. While this study has tackled the initial challenge of resolving the millimeter emission in these systems and relating it to the global disk structures, the real utility of these targets now lies with continued work that focuses on the details. For example, future observations of these disks with the *Atacama Large Millimeter Array* could be sensitive to the structural asymmetries or recently ejected material streams expected from non-coplanar tidal interactions (Akeson et al. 2007; Verrier & Evans 2008). However, it is equally important to calculate the stellar orbits in these nearby systems, particularly in the less-studied case of Hen 3-600. In fact, there are exciting opportunities to simultaneously refine the stellar orbits and directly probe star-disk interactions for the HD 98800 system, as the visual A-B binary will reach periastron in the next  $\sim 15$  years (Tokovinin 1999). Therefore, with continued monitoring the circumstellar material in the Hen 3-600 and HD 98800 systems can eventually serve as the primary observational calibrators for models of star-disk (as well as planet-disk) tidal interactions.

We are grateful to David Latham and Guillermo Torres for sharing their orbital expertise on these systems, and especially to Elise Furlan and the *Spitzer* GTO team lead by Dan Watson for kindly permitting the use of their calibrated IRS spectra. We thank the referee for an insightful review that helped improve the article. The SMA is a joint project between the Smithsonian Astrophysical Observatory and the Academia Sinica Institute of Astronomy and Astrophysics and is funded by the Smithsonian Institute and the Academia Sinica. Support for this work was provided by NASA through Hubble Fellowship grant HF-01203.01-A awarded by the Space Telescope Science Institute, which is operated by the Association of Universities for Research in Astronomy, Inc., for NASA, under contract NAS 5-26555. Partial support for I. C. was provided by the NSF REU and DOD ASSURE programs under NSF grant 0754568 and by the Smithsonian Institution. D. J. W. acknowledges support from NASA Origins grant NNG05GI81G. C. E. was supported by the National Science Foundation under award 0901947.

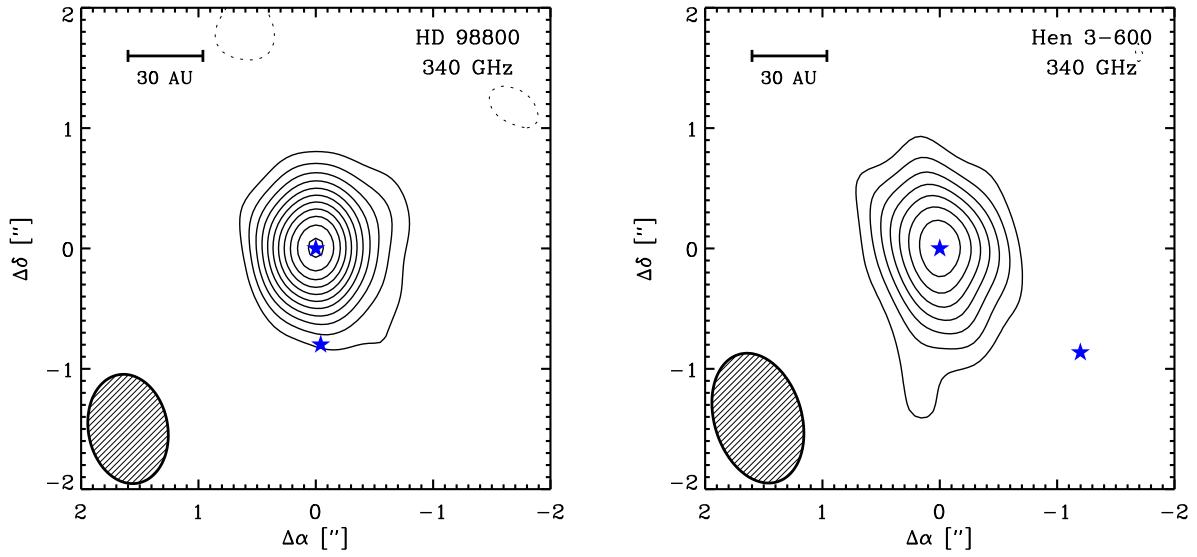


Fig. 1.— Aperture synthesis images of the  $880\ \mu\text{m}$  (340 GHz) dust continuum emission in the HD 98800 (*left*) and Hen 3-600 (*right*) multiple star systems. Contours start at  $3\sigma$  ( $10\ \text{mJy beam}^{-1}$ ) and are shown at  $2\sigma$  intervals. The synthesized beam dimensions are marked in the lower left corner of each image, and a 30 AU scale bar is included in the upper left. The images are centered at the peak of the continuum emission, corresponding to the positions of the HD 98800 B and Hen 3-600 A spectroscopic binaries. Each stellar component is marked with a blue star symbol.

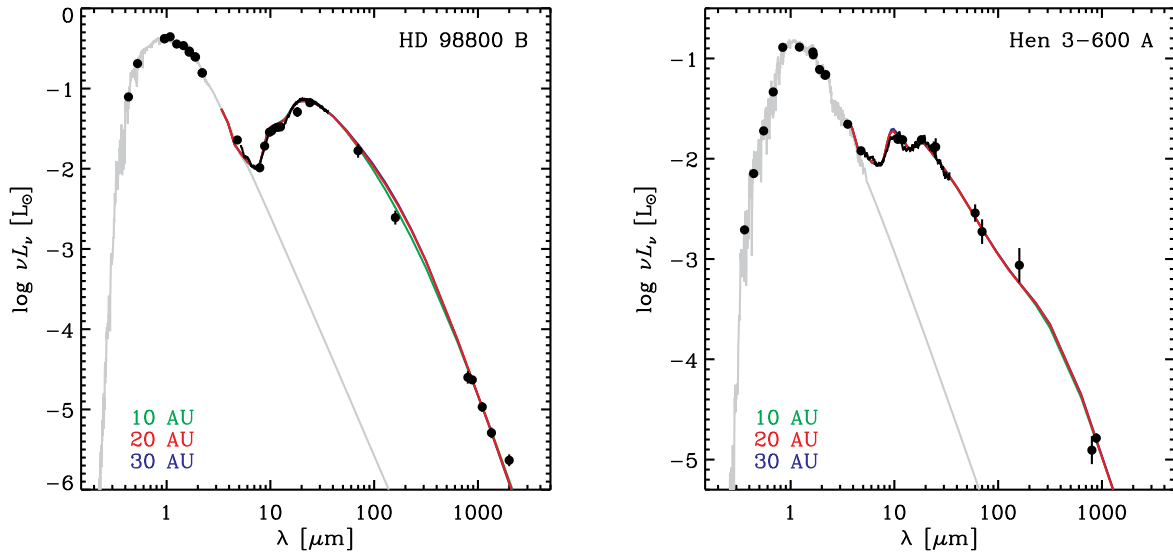


Fig. 2.— Broadband spectral energy distributions for the HD 98800 B (*left*) and Hen 3-600 A (*right*) disks, constructed from measurements in the literature. Light gray curves mark the composite stellar photospheres adopted for the radiative transfer modeling, while the black curves show the *Spitzer* IRS spectra corrected for the contamination of the nearby companions (see text). The overlaid curves are disk structure models for different values for the outer disk radius,  $R_{\text{out}}$ , as labeled in the lower left corner of each plot. The individual models are difficult to distinguish here, but show clear differences in terms of the  $880 \mu\text{m}$  visibilities (see Fig. 3).

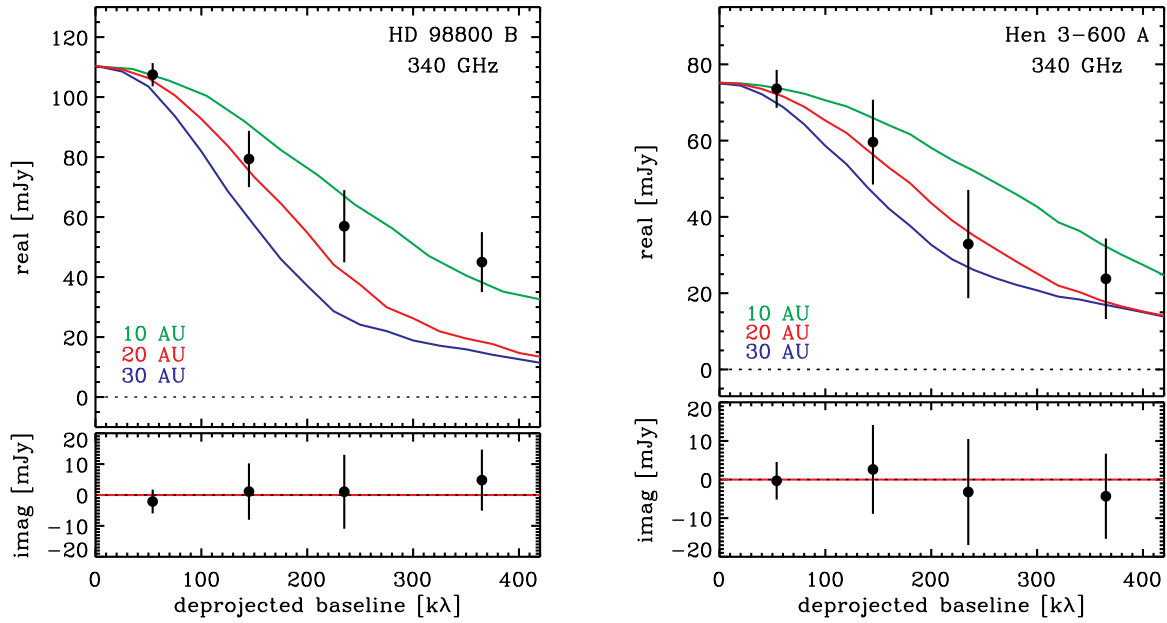


Fig. 3.— The azimuthally-averaged 880  $\mu\text{m}$  continuum visibilities (real and imaginary parts) as a function of the deprojected baseline length for the HD 98800 B (*left*) and Hen 3-600 A (*right*) disks. The overlaid curves are truncated disk structure models with different values for the outer edge radius,  $R_{\text{out}}$ , as labeled in the lower left corner of each plot.

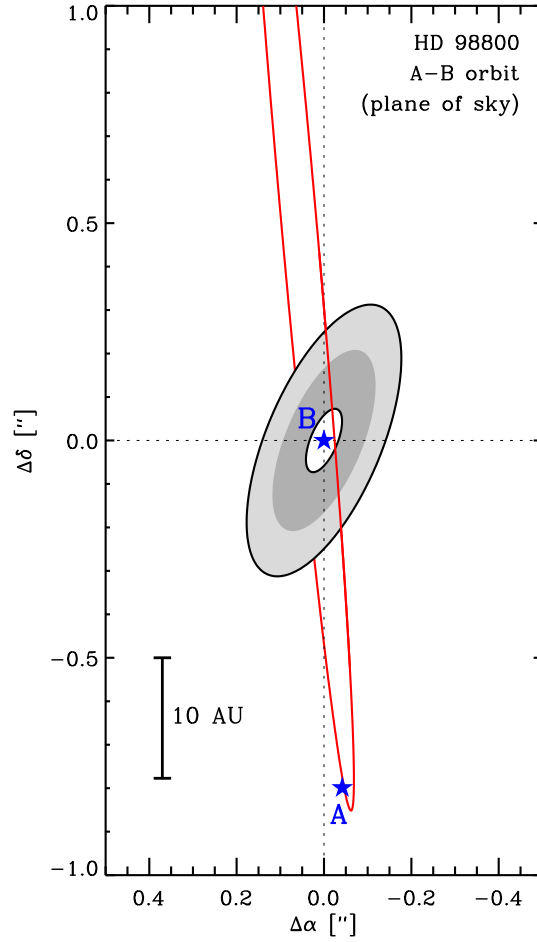


Fig. 4.— The inferred geometry of the HD 98800 B disk (*grayscale*) is compared with the A-B visual binary orbit (*red*) computed by Tokovinin (1999), projected onto the plane of the sky. The two-toned gray shading of the disk corresponds to the quoted range of possible  $R_{\text{out}}$  values ( $\sim 10$ -15 AU).

Table 1. Adopted Stellar Parameters

Star	$T_{\text{eff}}$ [K]	$R_*$ [ $R_{\odot}$ ]	$\log g$ [ $\text{cm s}^{-2}$ ]	$A_V$ [mags]
HD 98800 Aa+Ab	4500	1.30	4.00	0.0
HD 98800 Ba	4250	1.16	4.25	0.3
HD 98800 Bb	4000	0.90	4.25	0.3
Hen 3-600 Aa+Ab	3350	1.20	4.50	0.0
Hen 3-600 B	3350	1.00	4.50	0.0

Note. — The effective temperatures, radii, gravities, and extinctions determined for each stellar component, based on matching resolved optical/near-infrared photometry to scaled Lejeune et al. (1997) spectral templates. The parameters for HD 98800 B are based on the Boden et al. (2005) measurements: the templates were summed into a composite spectrum for the radiative transfer modeling. The  $A_V$  estimates correspond to the Mathis (1990) extinction law.



Table 2. Estimated Disk Parameters

Parameter	HD 98800 B	Hen 3-600 A
$R_{\text{in}}$ [AU]	2.0	0.4
$R_{\text{cav}}$ [AU]	3.5	1.0
$R_{\text{out}}$ [AU]	10-15	15-25
$M_{\text{dust}}$ [ $M_{\odot}$ ]	$3 \times 10^{-6}$	$7 \times 10^{-6}$
$\delta_{\Sigma}$	$\sim 1000$	$\sim 500$
$H_{10\text{AU}}$ [AU]	0.5	0.3
$\psi$	0.10	0.07
$\delta_H$	1.4	1.2
$f_{\text{sg}}$	0.25	0.10
$i$ [ $^{\circ}$ ]	67	36
PA [ $^{\circ}$ ]	158	169

Note. — Disk structure parameters estimated from the radiative transfer modeling. The parameter definitions are given in §4.

## REFERENCES

- Abt, H. A., Levy, S. G. 1976, *ApJS*, 30, 273
- Akeson, R. L., Koerner, D. W., & Jensen, E. L. N. 1998, *ApJ*, 505, 358
- Akeson, R. L., Rice, W. K. M., Boden, A. F., Sargent, A. I., Carpenter, J. M., & Bryden, G. 2007, *ApJ*, 670, 1240
- Andrews, S. M., & Williams, J. P. 2005, *ApJ*, 619, L175 (2005a)
- 2005, *ApJ*, 631, 1134 (2005b)
- 2007, *ApJ*, 659, 705 (2007a)
- 2007, *ApJ*, 671, 1800 (2007b)
- Andrews, S. M., Wilner, D. J., Hughes, A. M., Qi, C., & Dullemond, C. P. 2009, *ApJ*, 700, 1502
- Artymowicz, P., & Lubow, S. H. 1994, *ApJ*, 421, 651
- Bate, M. R., & Bonnell, I. A. 1997, *MNRAS*, 285, 33
- Bate, M. R. 2000, *MNRAS*, 314, 33
- Beckwith, S. V. W., Sargent, A. I., Chini, R. S., & Güsten, R. 1990, *AJ*, 99, 924
- Boden, A. F., et al. 2005, *ApJ*, 635, 442
- Brandeker, A., Jayawardhana, R., & Najita, J. 2003, *AJ*, 126, 2009
- Chiang, E. I., Joungh, M. K., Creech-Eakman, M. J., Qi, C., Kessler, J. E., Blake, G. A., & van Dishoeck, E. F. 2001, *ApJ*, 547, 1077
- Cutri, R. M., et al. 2003, *2MASS All-Sky Point Source Catalog* (Pasadena: IPAC)
- D’Alessio, P., et al. 2005, *ApJ*, 621, 461
- de la Reza, R., Torres, C. A. O., Quast, G., Castilho, B. V., & Vieira, G. L. 1989, *ApJ*, 343, L61
- Dent, W. R. F., Greaves, J. S., & Coulson, I. M. 2005, *MNRAS*, 359, 663
- Desidera, S., & Barbieri, M. 2007, *A&A*, 462, 345
- Dullemond, C. P., Dominik, C., & Natta, A. 2001, *A&A*, 560, 957
- Dullemond, C. P., & Dominik, C. 2004, *A&A*, 417, 159
- Dunkin, S. K., Barlow, M. J., & Ryan, S. G. 1997, *MNRAS*, 290, 165

- Duquennoy, A., & Mayor, M. 1991, *A&A*, 248, 485
- Furlan, E., et al. 2007, *ApJ*, 664, 1176
- Geoffroy, H., & Monin, J.-L. 2001, *A&A*, 369, 239
- Ghez, A. M., Neugebauer, G., & Matthews, K. 1993, *AJ*, 106, 2005
- Gregorio-Hetem, J., Lepine, J. R. D., Quast, G. R., Torres, C. A. O., & De La Reza, R. 1992, *AJ*, 103, 549
- Guilloteau, S., Dutrey, A., & Simon, M. 1999, *A&A*, 348, 570
- Guilloteau, S., Dutrey, A., Pety, J., & Gueth, F. 2008, *A&A*, 478, L31
- Ho, P. T. P., Moran, J. M., & Lo, K. Y. 2004, *ApJ*, 616, L1
- Holman, M. J., & Wiegert, P. A. 1999, *AJ*, 117, 621
- Huenemoerder, D. P., Kastner, J. H., Testa, P., Schulz, N. S., & Weintraub, D. A. 2007, *ApJ*, 671, 592
- Hughes, A. M., Wilner, D. J., Calvet, N., D’Alessio, P., Claussen, M. J., & Hogerheijde, M. R. 2007, *ApJ*, 664, 536
- Isella, A., & Natta, A. 2005, *A&A*, 438, 899
- Jayawardhana, R., Hartmann, L., Fazio, G., Fischer, R. S., Telesco, C. M., & Piña, R. K. 1999, *ApJ*, 520, L41
- Jensen, E. L. N., Mathieu, R. D., & Fuller, G. A. 1994, *ApJ*, 429, L29
- 1996, *ApJ*, 458, 312 (1996a)
- Jensen, E. L. N., Koerner, D. W., & Mathieu, R. D. 1996, *AJ*, 111, 2431 (1996b)
- Jensen, E. L. N., & Mathieu, R. D. 1997, *AJ*, 114, 301
- Jensen, E. L. N., & Akeson, R. L. 2003, *ApJ*, 584, 875
- Kastner, J. H., Zuckerman, B., Weintraub, D. A., & Forveille, T. 1997, *Science*, 277, 67
- Kastner, J. H., Huenemoerder, D. P., Schulz, N. S., Canizares, C. R., Li, J., & Weintraub, D. A. 2004, *ApJ*, 605, L49
- Koerner, D. W., Jensen, E. L. N., Cruz, K. L., Guild, T. B., & Gultekin, K. 2000, *ApJ*, 533, L37
- Lada, C. J. 2006, *ApJ*, 640, L63
- Lay, O. P., Carlstrom, J. E., & Hills, R. E. 1997, *ApJ*, 489, 917

- Leinert, C., et al. 1993, *A&A*, 278, 129
- Lejeune, T., Cuisinier, F., & Buser, R. 1997, *A&A*, 125, 229
- Lin, D. N. C., & Papaloizou, J. 1993, in *Protostars & Planets III*, eds. E. Levy & M. S. Matthews (Tucson: Univ. Arizona Press), 749
- Low, F. J., Hines, D. C., & Schneider, G. 1999, *ApJ*, 520, L45
- Low, F. J., Smith, P. S., Werner, M., Chen, C., Krause, V., Jura, M., & Hines, D. C. 2005, *ApJ*, 631, 1170
- Mathieu, R. D., Ghez, A. M., Jensen, E. L. N., & Simon, M. 2000, in *Protostars & Planets IV*, eds. V. Mannings, A. P. Boss, & S. S. Russell (Tucson: Univ. Arizona Press), 703
- Mathis, J. S. 1990, *ARA&A*, 28, 37
- Muzerolle, J., Calvet, N., Briceño, C., Hartmann, L., & Hillenbrand, L. 2000, *ApJ*, 535, L47
- Nagel, E., D'Alessio, P., Calvet, N., Espaillat, C., Sargent, B., Hernández, J., & Forrest, W. J. 2009, *ApJ*, in press
- Osterloh, M., & Beckwith, S. V. W. 1995, *ApJ*, 439, 288
- Patience, J., Akeson, R. L., & Jensen, E. L. N. 2008, *ApJ*, 677, 616
- Perryman, M. A. C., et al. 1997, *A&A*, 323, L49
- Pichardo, B., Sparke, L. S., & Aguilar, L. A. 2005, *MNRAS*, 359, 521
- 2008, *MNRAS*, 391, 815
- Pierens, A., & Nelson, R. P. 2008, *A&A*, 483, 633
- Prato, L., et al. 2001, *ApJ*, 549, 590
- Raghavan, D., Henry, T. J., Mason, B. D., Subsavane, J. P., Jao, W.-C., Beaulieu, T. D., & Hambly, N. C. 2006, *ApJ*, 646, 523
- Reipurth, B., & Zinnecker, H. 1993, *A&A*, 278, 81
- Salyk, C., Blake, G. A., Boogert, A. C. A., & Brown, J. M. 2009, *ApJ*, 699, 330
- Simon, M., et al. 1995, *ApJ*, 443, 625
- Soderblom, D. R., et al. 1998, *ApJ*, 498, 385
- Sylvester, R. J., Skinner, C. J., Barlow, M. J., & Mannings, V. 1996, *MNRAS*, 279, 915
- Sylvester, R. J., Dunkin, S. K., & Barlow, M. J. 2001, *MNRAS*, 327, 133

- Thamm, E., Steinacker, J., & Henning, T. 1994, *A&A*, 287, 493
- Tokovinin, A. A. 1999, *Astronomy Letters*, 25, 669
- Torres, G., Stefanik, R. P., Latham, D. W., & Mazeh, T. 1995, *ApJ*, 452, 870
- Torres, G., Guenther, E. W., Marschall, L. A., Neuhäuser, R., Latham, D. W., & Stefanik, R. P. 2003, *AJ*, 125, 825
- Torres, C. A. O., Quast, G. R., Da Silva, L., de la Reza, R., Melo, C. H. F., & Sterzik, M. 2006, *A&A*, 460, 695
- Uchida, K. I., et al. 2004, *ApJS*, 154, 439
- van Leeuwen, F. 2007, *A&A*, 474, 653
- Verrier, P. E., & Evans, N. W. 2008, *MNRAS*, 390, 1377
- Webb, R. A., Zuckerman, B., Platais, I., Patience, J., White, R. J., Schwartz, M. J., & McCarthy, C. 1999, *ApJ*, 512, L63
- Weintraub, D. A., Saumon, D., Kastner, J. H., & Forveille, T. 2000, *ApJ*, 530, 867